Orchestrating Medical Image Compression and Remote Segmentation Networks

Zihao Liu[1,2(✉)], Sicheng Li[2], Yen-kuang Chen[2], Tao Liu[1], Qi Liu[3], Xiaowei Xu[4], Yiyu Shi[4], and Wujie Wen[3]

[1] FIU, Miami, FL, USA
zliu021@fiu.edu
[2] Alibaba DAMO Academy, Hangzhou, China
[3] Lehigh University, Bethlehem, PA, USA
[4] University of Notre Dame, Notre Dame, IN, USA

Abstract. Deep learning-based medical image segmentation on the cloud offers superb performance by harnessing the recent model innovation and hardware advancement. However, one major factor that limits its overall service speed is the long data transmission latency, which could far exceed the segmentation computation time. Existing image compression techniques are unable to achieve an efficient compression to dramatically reduce the data offloading overhead, while maintaining a high segmentation accuracy. The underlying reason is that they are all developed upon human visual system, whose image perception pattern could be fundamentally different from that of deep learning-based image segmentation. Motivated by this observation, in this paper, we propose a generative segmentation architecture consisting of a compression network, a segmentation network and a discriminator network. Our design orchestrates and coordinates segmentation and compression for simultaneous improvements of segmentation accuracy and compression efficiency, through a dedicated GAN architecture with novel loss functions. Experimental results on 2D and 3D medical images demonstrate that our design can reduce the bandwidth requirement by 2 orders-of-magnitude comparing with that of uncompressed images, and increase the accuracy of remote segmentation remarkably over the state-of-the-art solutions, truly accelerating the cloud-based medical imaging service.

1 Introduction

Recent advances in deep learning have significantly boosted the performance of automatic medical image segmentations [6,7,9,13,22,26,31]. However, such methods usually incur extremely high computational cost [36]. For example, segmenting a 3D Computed Tomography (CT) volume with a typical neural

Electronic supplementary material The online version of this chapter (https://doi.org/10.1007/978-3-030-59719-1_40) contains supplementary material, which is available to authorized users.

A. L. Martel et al. (Eds.): MICCAI 2020, LNCS 12264, pp. 406–416, 2020.
https://doi.org/10.1007/978-3-030-59719-1_40

network [5] involves 2.2 Tera floating-point operations (TFLOPs), making the real-time service impossible with a resource-constraint local computing device. The problem becomes more prominent considering the exponentially growing number of medical images in the past decade [12]. A viable solution is to have the cloud computing platforms to conduct the deep learning-based analyses [21,38,39].

However, the modern medical imaging requires significantly large data volume to represent high resolution and graphical fidelity, posing severe challenges on the data transmission from the local to the cloud. The latency overhead brought by such data transmission could be much longer than that of deep learning computations which are accelerated by clusters of GPUs, hence dominates the overall service time [18]. For example, as long as 13 s are required to transmit one 3D CT image of size 300 MB [24], whereas the state-of-the-art segmentation network only takes about a hundred milliseconds to process on the cloud [11,16,20].

A common practice to lower such excessive data transfer overhead would be image compression. While many popular standards like JPEG [34], JPEG-2000 [2,3], MPEG [15], as well as their enhanced versions [4,19,27,28,35], can partially address this issue, the achievable compression rate improvement is limited because all the solutions need to guarantee the image's visual quality for human eyes, rather than deep learning systems. Image compression using neural network-based auto-encoders [1,8,17,23,33] can surpass aforementioned standards, however, the underlying constraint is still the human perceived image quality measurement like PNSR and SSIM, instead of deep learning accuracy. The most recent work [33] proposed to directly use the compressed representation from the encoder to accelerate the computation of image classification and segmentation, unfortunately, there exist two drawbacks which make such a solution very impractical on medical imaging: 1) limited compression rate due to its focus on minimizing the pixel-wise difference between original image and reconstruct image; 2) unacceptable accuracy loss comparing with that of uncompressed images. Apparently, almost all the above compression methods are designed to minimize the human visual distortion, however, when processing image at the cloud side the image quality is usually judged by network performance (e.g., segmentation accuracy) rather than human vision. As a result, it naturally brings up several interesting questions: *1) Can we design a compression method optimal for deep learning-based image segmentation instead of human vision? 2) If so, how should we design that? Is it possible to design a* ***matched*** *pair of compression and segmentation network for the whole process? Will the achievable compression rate and segmentation quality under such a method outperform the existing solutions significantly?*

In this work, we propose to orchestrate medical image compression and segmentation networks for efficient data transmission as well as high segmentation accuracy. Particularly, our end-to-end method trains multiple neural networks simultaneously for both image compression locally and segmentation in the cloud using adversarial learning, thus to make the two steps matched to extract and retain the most important features for segmentation. The neural network for

image compression is designed to be light-weighted, which fits well for local processing. The main contributions of our work are as follows: 1) We propose a joint method to integrate the compression network and the generative segmentation network (with a discriminator network), so as to fully unleash the compression potential on medical imaging; 2) We design a series of training loss functions to optimize the compressive segmentation in the proposed network architecture, to achieve high compression rate while maintaining the segmentation accuracy; 3) We conduct comprehensive evaluations on 2D and 3D medical images and report that our method outperforms latest solutions in two aspects: for the same compression rate, our method achieves better segmentation accuracy; for the same level of segmentation accuracy, it offers remarkable compression rate improvement compared with the state-of-the-art designs. These advantages demonstrate great potentials for its applications in today's deep neural network assisted medical image segmentation.

2 Method

Figure 1 depicts an overview of our proposed design, which consists of three integrated components: the compression network (C), the segmentation network (S) and the discrimination network (D). Specifically, 1) C functions as a lossy image compression engine to ensure efficient data transmission. Also, the compression network should be light-weighted for fast processing on resource-constraint local computing devices; 2) The segmentation network S could be any commonly-used segmentor s with feature reconstruction layers g. Instead of reconstructing the whole image, g only reconstructs the essential feature maps that will be used to generate a probability label map by segmentor. 3) The discriminator D aims to capture any difference between the predicted label map from S and the corresponding ground truth label map. C, S and D are alternatively trained in an adversarial fashion by solving a min-max optimization problem. The goal is to achieve a high compression ratio, under the guidance of DNN-based segmentation quality measurement (NOT human perceived image quality), so as to facilitate data transmission while providing similar or even higher segmentation accuracy for better Quality-of-Service (QoS).

Note that the compressed bitstream sent to the cloud will be only used by segmentation networks in order to generate accurate segmentation label maps. Such predicted label maps, together with the local stored high-resolution image copies, will assist doctors for medical diagnosis, surgical planning/treatment etc. Therefore, the compression network does not necessarily preserve high image visual quality, but to guarantee the correct segmentation results.

2.1 Network Architecture Design

Compression Network (C): Unlike the existing neural network-based compression methods which attempt to minimize the pixel-wise visual distortions between original image and reconstructed image, our compression network

focuses on minimizing the difference between the predict label from S and ground truth label y for an input x, as well as the number of required bits ($-log_2Q(C(x))$, where Q is a probabilistic model described in Sect. 2.2). This indicates that C is dedicated to compress images in an DNN-favorable manner to filter out the undesired features and aggressively improve the compression ratio. Figure 2(a) shows the detailed network architecture to compress 2D medical images. The compression network for 3D images is designed following the similar approach. To generate a lightweight network for efficient local processing, we limit model parameters by reducing the number of feature maps at each layer or directly dropping some convolutional layers The network profiling on the number of parameters and the number of computations required by C is 1.3 M and 8.1 GFLOPs, which are only 0.83% and 0.79% as that of a segmentation network [37]. For more details, please see our supplemental material.

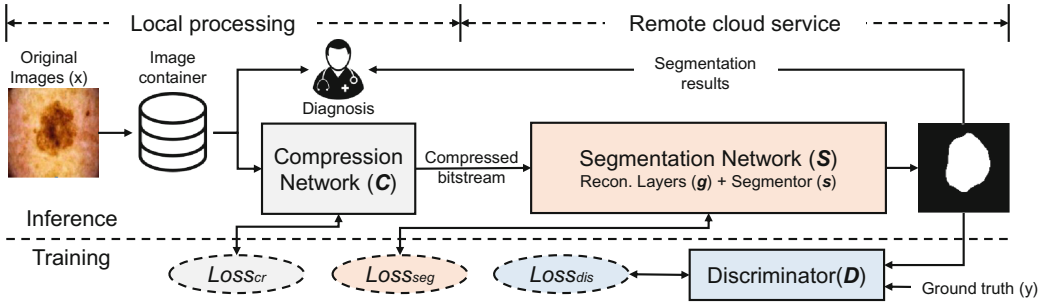

Fig. 1. Orchestrated medical image compression and remote segmentation networks.

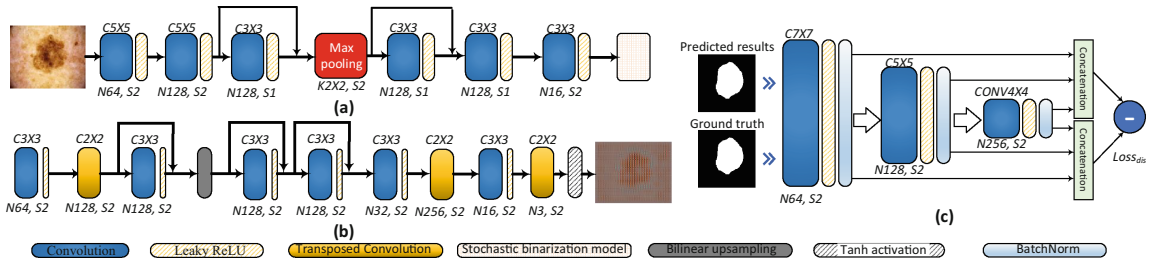

Fig. 2. Illustrations of (a) Compression network; (b) Feature reconstruction layers and (c) Discriminator network in our design.

Segmentation Network (S) and Discriminator (D): We do not intentionally design new segmentors, instead, we adopt existing representative networks for 2D and 3D segmentation tasks [14,37] so as to demonstrate the scalability of our design. For this purpose, we add the feature reconstruction layers (g) to ensure the output from compression network is compatible with any s. Note that our g does not try to reconstruct the whole detailed image, but features required information for s. Figure 2(b) illustrates the detail network structure. To further compensate the potential accuracy loss caused by the joint training of S and C, our method incorporates a discriminator D after the S, shown as

Fig. 2(c). The ground truth label map and predicted label map from S will be fed into D one by one, the output from each layer will concatenate together and then their difference will be used as the label feature loss to train C, S and D. One thing we'd emphasise is that the D is also segmentation accuracy guided, it only distinguish the label maps rather than the image quality, which is totally different from the previous works.

2.2 Training Loss Design

After determining the network architectures, we now design the loss function dedicated to each network for jointly training. Given a dataset with N training images x_n, and y_n as the corresponding ground truth label map, the multi-scale label feature loss ($loss_{dis}$) and segmentation loss ($loss_{seg}$) can be defined as follows:

$$loss_{dis} = \min_{\theta_C,\theta_S} \max_{\theta_D} \zeta(\theta_C, \theta_S, \theta_D) = \frac{1}{N} \sum_{n=1}^{N} \ell_{mae}(\phi_D(\phi_S(\phi_C(x_n))), \phi_D(y_n)) \quad (1)$$

$$loss_{seg} = \min_{\theta_C,\theta_S} \xi(\theta_C, \theta_S) = \ell_{mse}(\phi_S(\phi_C(x_n)), y_n) \quad (2)$$

where θ_C, θ_S and θ_D are weight parameters of C, S and D, respectively. ℓ_{mae} is the mean absolute error or L_1 distance inspired by [37], $\phi_S(\phi_C(x_n))$ is the prediction result of S after input x_n is compressed by compression network C and $\phi_D(\cdot)$ represents the multi-scale hierarchical features extracted from each convolutional layer in D. ℓ_{mse} is the MSE between predicted label from S and ground truth label. $\phi_C(\cdot)$, $\phi_S(\cdot)$ and $\phi_D(\cdot)$ represent the functionality of C, S and D, respectively. Thus, the loss for the discriminator is formulated as:

$$-loss_{dis} = -\min_{\theta_C,\theta_S} \max_{\theta_D} \zeta(\theta_C, \theta_S, \theta_D) \quad (3)$$

We set this loss with a negative value to maximize the difference between the predicted label and the ground truth label. On the contrary, we add the reserved version of this loss (positive value) to C and S, with the goal of minimizing such loss for the combined C and S. Therefore, the total loss for segmentor and compression network is:

$$loss_{total} = loss_{dis} + loss_{seg} = \min_{\theta_C,\theta_S} \xi(\theta_C, \theta_S) + \min_{\theta_C,\theta_S} \max_{\theta_D} \zeta(\theta_C, \theta_S, \theta_D) \quad (4)$$

Finally, we introduce a compression loss ($loss_{cr}$) to optimize the output of C for achieving the best compression rate. We use e to estimate the number of bits for the representation after C, e.g. entropy coding. Since this coding process is non-differentiable, we adopt a continuous differentiable Jensen's inequality [29] to estimate the upper bound of the number of required bits. This estimation is used to train the compression network [30]. Then the total loss for C is:

$$loss_{cr} + loss_{seg} + loss_{dis} = \underbrace{min(e(f(x_n)))}_{\#\ of\ bits} + \underbrace{\min_{\theta_C,\theta_S} \max_{\theta_D} \zeta(\theta_C, \theta_S, \theta_D) + \min_{\theta_C,\theta_S} \xi(\theta_C, \theta_S)}_{Segmentation\ distortion} \quad (5)$$

2.3 Training and Testing

Our training process follows an alternating fashion: for each training epoch, **1)** we fix the parameters of D and only train that of C and S for one step using above designed loss functions, i.e. $loss_{total}$ (Eq. 4) for g and segmentor s, and C has an extra loss $loss_{cr}$ (Eq. 5) to optimize the compression rate; Note that a stochastic binarization algorithm [32] is applied to the encoded data, i.e. the compressed representation is in binary format. **2)** We fix the parameters of C and S then train D by the gradients computed from its loss function ($loss_{dis}$). As Eq. 1 shows, this training process behaves more like a min-max game: while C and S try to minimize $loss_{dis}$, D attempts to maximize it. As a result, the network training gradually improves the segmentation results of S, as well as the compression efficiency of C after each epoch until reaching convergence. At the testing process, only C and S are used to predict the segmentation label maps and D is not involved.

3 Experiments and Results

3.1 Experimental Setup

Dataset. We use ISIC 2017 challenge dataset [10] to evaluate the 2D image segmentation. This fully annotated dataset provides 2000 training images, 150 validation images for the Lesion segmentation task. For 3D image segmentation, we select the HVSMR 2016 challenge dataset [25], which consists of 5 3D cardiac MR scans for training and 5 scans for testing. Each image includes three segmentation labels: myocardium, blood pool and background. Note that directly training with the large-size 3D medical images is not feasible, instead, we randomly crop the original image to many smaller pieces of data to facilitate training and overcome the overfitting, which is consistent with [18].

Target Designs. Our network architectures are realized by heavily modifying the adversarial segmentation network from SegAN [37] and incorporating our compression network, replacing the discriminator network, etc. Specifically, our networks include: ***D1*** with only segmentator S and discriminator D; ***D2*** with compression network C and segmentation network S but no discriminator; ***D3*** with all of the compression network C, segmentation network S and discriminator D, without considering the compression loss. This design is expected to offer the best segmentation accuracy, but limited compression efficiency; ***D4*** with compression loss upon ***D3***. This design should achieve aggressive compression rate with slightly degraded segmentation accuracy. For a fair comparison, we adopt the traditional JPEG-2000, H.264, the auto encoder-based and the latest machine vision-based compression [18] in our evaluations. Note that the auto encoder-based compression (Auto/Seg) is implemented to reconstruct original image for segmentor. As such, we expect Auto/Seg should suffer from prominent segmentation accuracy loss at high compression rates. All the methods are evaluated under four aspects: *segmentation performance, compression efficiency, cloud-based service latency and visual analysis.*

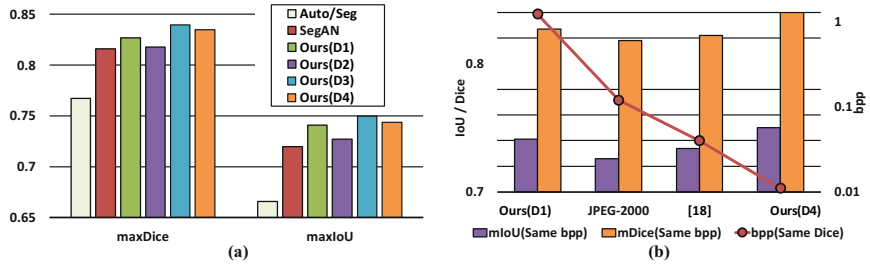

Fig. 3. (a) Segmentation results under different network configurations. (b) Segmentation accuracy and bpp comparisons with prior methods.

Table 1. 3D segmentation results on HVSMR 2016 challenge dataset [25]

	Myocardium						Blood pool					
	Dice			IoU			Dice			IoU		
	Uncomp.	[18]	Ours	Uncomp.	[18]	Ours	Uncomp.	[18]	Ours	Uncomp.	[18]	Ours
Img.1	0.895	0.868	0.899	0.809	0.756	0.817	0.915	0.876	0.927	0.844	0.818	0.864
Img.2	0.829	0.798	0.831	0.708	0.681	0.711	0.951	0.903	0.948	0.916	0.875	0.921
Img.3	0.811	0.782	0.815	0.672	0.652	0.674	0.883	0.858	0.888	0.807	0.754	0.808
Img.4	0.877	0.853	0.874	0.780	0.758	0.776	0.955	0.906	0.956	0.913	0.872	0.915
Img.5	0.809	0.778	0.810	0.679	0.647	0.681	0.883	0.849	0.881	0.806	0.779	0.788
Average	0.844	0.816	**0.846**	0.729	0.699	**0.732**	0.918	0.878	**0.920**	0.857	0.820	**0.859**
bpp	Uncompressed (∼1.1)			H.264 (∼0.15)			[18](∼0.04)			**Ours(∼0.014)**		

3.2 Evaluation Results

2D Segmentation. Figure 3(a) reports the Dice/IoU score of 2D segmentation on the selected designs with different architectures and component combinations. Our methods, instead of degrading any accuracy, can even improve the segmentation performance after image compression. In particular, ***D1*** achieves higher score over SegAN, indicating that the proposed predict-oriented discriminator can better improve the segmentation accuracy with the combination of $Loss_{seg}$ and $Loss_{dis}$ than the baseline adversarial segmentation network on uncompressed images. With the consideration of compression, ***D3*** and ***D4*** shows the best Dice and IoU. This is because our joint training process attempts to learn as many features as possible with the compression network, segmentation network and discriminator. As expected, Auto/Seg, which is designed under the guidance of human visual quality loss (e.g. MSE), achieves the lowest Dice/IoU among all the methods. Figure 3(b) shows the average bpp (bits per pixel) of each compression approaches. ***D4*** which is trained with additional compression loss $Loss_{cr}$, gives the best average bpp of 0.012. That is to say, our method significantly improves the image compression rate by almost two orders of magnitude than that of uncompressed images (average bpp of 1.24), by one order of magnitude than that of JPEG-2000 (average bpp of 0.12) and >3× than that of the latest [18] (average bpp of 0.04).

3D Segmentation. Table 1 shows the evaluation results on 3D image segmentation. We test 3D CMR volumes with segmentation targets "Myocardium" and

"Blood Pool", and compare the Dice/IoU scores with the uncompressed design and the method in [18]. For a fair comparison, we keep the compression rate at the same level as ours (bpp = 0.014). Compared with the uncompressed image segmentation, our design improves the average Dice/IoU score by 0.002/0.003 and 0.002/0.002 on "Myocardium" and "Blood Pool", respectively. Moreover, we demonstrate a significant improvement on Dice/IoU score comparing with the latest work [18], for the reason that this method cannot keep high segmentation accuracy at a high compression rate. These results show great scalability and outstanding segmentation performance of our design for 3D images.

Cloud-Based Service Latency. Table 2 shows a detailed latency breakdown to process a 3D CT image of size 300 MB. The computation latency on the cloud is evaluated by Nvidia GeForce GTX 1080 GPUs, while the image compression runs on an Intel Core i7-6850 CPU to emulate a resource-constraint local computing device and the data transmission speed is retrieved from [24]. Putting them together, our design only takes a total latency of 0.26s, which achieves 5.7× and 2.4× speedup over the JPEG-based design and [18], respectively. Since the data transmission time dominates the total service latency, significantly improving compression rate with our solution is essential for service speedup. Considering the impressive performance and low compression overhead, our solution will be very attractive for ever-increasing DNN based medical image analyses.

Table 2. Latency breakdown of the cloud-based service

	Volume(MB)	Trans.(s)	Compression(s)	Reconstruction(s)	Segmentation(s)	Total(s)
JPEG	30	1.4	0.0013	0.0013	0.1	1.5026
[18]	10	0.53	0.0015	0.0015	0.1	0.633
Ours	3.3	0.16	0.003	0.0003	0.1	0.2633

Visual Analysis. The second row from Fig. 4 represents the visualization results from feature reconstruction layers g before feeding into a segmentor s. Compared with original images, the reconstructed feature maps preserve limited visual quality for human vision, however guarantee a correct segmentation. These results also indicate that: 1) the original images with RGB channels or with an intensity channel are not always the optimal, instead, our single-channel reconstructed feature maps fit well with the segmentation tasks. 2) some undesired features have been removed. For example, the hairs in the original image of first column are eliminated, which actually make the segmentations more accurate. 3) all the reconstructed feature maps from both 2D or 3D images, are formed by many small blocks with the same patterns and such patterns can further improve compression rate.

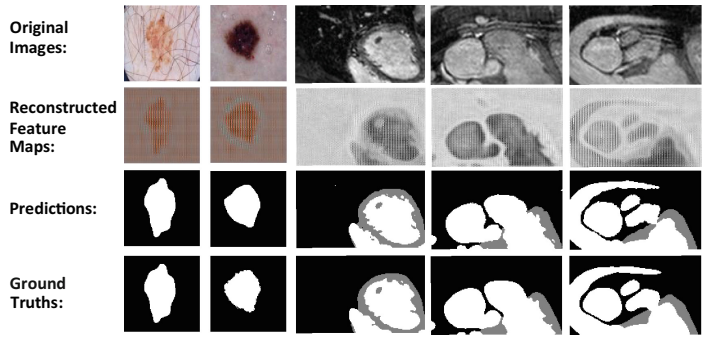

Fig. 4. The comparison between original images from 2D RGB dataset (left 2 columns) and 3D cardiovascular magnetic resonance (CMR) dataset (right 3 columns), reconstructed feature maps from feature reconstruction layers and the corresponding predicted label maps and ground truth label maps.

4 Conclusion

This work presents a generative segmentation architecture for compressed medical images. We propose to leverage the compression network and different loss function designs to enhance the cloud-based segmentation performance and efficiency by synthetically considering segmentation accuracy and compression rate. We conducted comprehensive evaluations on both 2D RGB and 3D CMR images and compared our design with state-of-the-art solutions. Experimental results show that our design not only significantly improves compression rate, but also increases the segmentation accuracy, outperforming the existing solutions by offering better efficiency on cloud-based image segmentation.

Acknowledgement. This work was supported in part by NSF Grants SPX-2006748 and SHF-2011236.

References

1. Agustsson, E., et al.: Generative adversarial networks for extreme learned image compression. arXiv:1804.02958 (2018)
2. Boliek, M.: Information technology JPEG 2000 image coding system: extensions for three-dimensional data. ISO/IEC 15444-10, ITU-T Rec. T.809 (2002)
3. Boliek, M.: JPEG 2000 image coding system: core coding system. ISO/IEC (2002)
4. Bruylants, T., et al.: Wavelet based volumetric medical image compression. Signal Process. Image Commun. **31**, 112–133 (2015)
5. Chen, J., et al.: Combining fully convolutional and recurrent neural networks for 3D biomedical image segmentation. In: Advances in Neural Information Processing Systems, pp. 3036–3044 (2016)
6. Chen, H., et al.: Deep contextual networks for neuronal structure segmentation. In: AAAI, pp. 1167–1173 (2016)
7. Chen, H., et al.: VoxResNet: deep voxelwise residual networks for brain segmentation from 3D MR images. NeuroImage **170**, 446–455 (2017)

8. Cheng, Z., Sun, H., Takeuchi, M., Katto, J.: Learning image and video compression through spatial-temporal energy compaction. In: Proceedings of the IEEE Conference on Computer Vision and Pattern Recognition, pp. 10071–10080 (2019)
9. Çiçek, Ö., Abdulkadir, A., Lienkamp, S.S., Brox, T., Ronneberger, O.: 3D U-Net: learning dense volumetric segmentation from sparse annotation. In: Ourselin, S., Joskowicz, L., Sabuncu, M.R., Unal, G., Wells, W. (eds.) MICCAI 2016. LNCS, vol. 9901, pp. 424–432. Springer, Cham (2016). https://doi.org/10.1007/978-3-319-46723-8_49
10. Codella, N.C., et al.: Skin lesion analysis toward melanoma detection: a challenge at the 2017 international symposium on biomedical imaging (ISBI), hosted by the international skin imaging collaboration (ISIC). In: 2018 IEEE 15th International Symposium on Biomedical Imaging (ISBI 2018), pp. 168–172. IEEE (2018)
11. Coomans, W., et al.: XG-fast: the 5th generation broadband. IEEE Commun. Mag. **53**(12), 83–88 (2015)
12. Dinov, I.D.: Volume and value of big healthcare data. J. Med. Stat. Inf. **4** (2016)
13. Dou, Q., Chen, H., Jin, Y., Yu, L., Qin, J., Heng, P.-A.: 3D deeply supervised network for automatic liver segmentation from CT volumes. In: Ourselin, S., Joskowicz, L., Sabuncu, M.R., Unal, G., Wells, W. (eds.) MICCAI 2016. LNCS, vol. 9901, pp. 149–157. Springer, Cham (2016). https://doi.org/10.1007/978-3-319-46723-8_18
14. Isensee, F., et al.: NNU-net: breaking the spell on successful medical image segmentation. arXiv preprint arXiv:1904.08128 (2019)
15. ITU-T, JTC: Generic coding of moving pictures and associated audio information-part 2: video (1995)
16. Kang, Y., et al.: Neurosurgeon: collaborative intelligence between the cloud and mobile edge. ACM SIGPLAN Notices **52**(4), 615–629 (2017)
17. Lee, J., Cho, S., Beack, S.K.: Context-adaptive entropy model for end-to-end optimized image compression. arXiv preprint arXiv:1809.10452 (2018)
18. Liu, Z., et al.: Machine vision guided 3d medical image compression for efficient transmission and accurate segmentation in the clouds. In: Conference on Computer Vision and Pattern Recognition (2019)
19. Liu, Z., et al.: DeepN-JPEG: a deep neural network favorable JPEG-based image compression framework. In: Proceedings of the 55th Annual Design Automation Conference, pp. 1–6 (2018)
20. Ma, Y., Jia, Z.: Evolution and trends of broadband access technologies and fiber-wireless systems. In: Tornatore, M., Chang, G.-K., Ellinas, G. (eds.) Fiber-Wireless Convergence in Next-Generation Communication Networks, pp. 43–75. Springer, Cham (2017). https://doi.org/10.1007/978-3-319-42822-2_2
21. Marwan, M., et al.: Using cloud solution for medical image processing: issues and implementation efforts. In: 2017 3rd International Conference of Cloud Computing Technologies and Applications (CloudTech), pp. 1–7. IEEE (2017)
22. Milletari, F., et al.: V-net: fully convolutional neural networks for volumetric medical image segmentation. In: 2016 Fourth International Conference on 3D Vision (3DV), pp. 565–571. IEEE (2016)
23. Minnen, D., et al.: Joint autoregressive and hierarchical priors for learned image compression. In: Advances in Neural Information Processing Systems, pp. 10771–10780 (2018)
24. Molla, R.: Fixed broadband speeds are getting faster - what's fastest in your city? (2017)

25. Pace, D.F., Dalca, A.V., Geva, T., Powell, A.J., Moghari, M.H., Golland, P.: Interactive whole-heart segmentation in congenital heart disease. In: Navab, N., Hornegger, J., Wells, W.M., Frangi, A.F. (eds.) MICCAI 2015. LNCS, vol. 9351, pp. 80–88. Springer, Cham (2015). https://doi.org/10.1007/978-3-319-24574-4_10
26. Ronneberger, O., Fischer, P., Brox, T.: U-Net: convolutional networks for biomedical image segmentation. In: Navab, N., Hornegger, J., Wells, W.M., Frangi, A.F. (eds.) MICCAI 2015. LNCS, vol. 9351, pp. 234–241. Springer, Cham (2015). https://doi.org/10.1007/978-3-319-24574-4_28
27. Sanchez, V., et al.: 3-D scalable medical image compression with optimized volume of interest coding. IEEE Trans. Med. Imaging **29**(10), 1808–1820 (2010)
28. Sanchez, V., Abugharbieh, R., Nasiopoulos, P.: Symmetry-based scalable lossless compression of 3D medical image data. IEEE Trans. Med. Imaging **28**(7), 1062–1072 (2009)
29. Theis, L., et al.: A note on the evaluation of generative models. arXiv preprint arXiv:1511.01844 (2015)
30. Theis, L., et al.: Lossy image compression with compressive autoencoders. arXiv preprint arXiv:1703.00395 (2017)
31. Wang, T., et al.: SCNN: a general distribution based statistical convolutional neural network with application to video object detection. In: The Thirty-Third AAAI Conference on Artificial Intelligence (AAAI 2019) (2019)
32. Toderici, G., et al.: Variable rate image compression with recurrent neural networks. arXiv preprint arXiv:1511.06085 (2015)
33. Torfason, R., et al.: Towards image understanding from deep compression without decoding. arXiv preprint arXiv:1803.06131 (2018)
34. Wallace, G.K.: The JPEG still picture compression standard. IEEE Trans. Consum. Electron. **38**(1), xviii–xxxiv (1992)
35. Xu, Z., et al.: Diagnostically lossless coding of X-ray angiography images based on background suppression. Comput. Electr. Eng. **53**, 319–332 (2016)
36. Xu, X., et al.: Scaling for edge inference of deep neural networks. Nat. Electron. **1**(4), 216 (2018)
37. Xue, Y., et al.: Segan: adversarial network with multi-scale L1 loss for medical image segmentation. Neuroinformatics **16**(3–4), 383–392 (2018)
38. Zhao, T., et al.: Cloud-based medical image processing system with anonymous data upload and download, US Patent 8,553,965, 8 October 2013
39. Zhao, T., et al.: Cloud-based medical image processing system with access control, US Patent 8,682,049, 25 March 2014